BIOCHEMISTRY
including biophysical chemistry & molecular biology
Article

Biochemistry **2010,** *49,* 2925–2931 2925
DOI: 10.1021/bi9021439

Membrane Topological Analysis of the Proton-Coupled Folate Transporter (PCFT-SLC46A1) by the Substituted Cysteine Accessibility Method†

Rongbao Zhao, Ersin Selcuk Unal,‡ Daniel Sanghoon Shin, and I. David Goldman*

Departments of Medicine and Molecular Pharmacology, Albert Einstein College of Medicine, 1300 Morris Park Avenue, Bronx, New York 10461. ‡Current address: Department of Surgery, University of Istanbul, Istanbul, Turkey.

Received December 14, 2009; Revised Manuscript Received February 16, 2010

ABSTRACT: The proton-coupled folate transporter (PCFT) mediates intestinal folate absorption. Loss-of-function mutations in this gene are the molecular basis for the autosomal recessive disorder, hereditary folate malabsorption. In this study, the substituted cysteine accessibility method was utilized to localize extra- or intracellular loops connecting predicted PCFT transmembrane domains. Cysteine-less PCFT was generated by replacement of all seven cysteine residues with serine and was shown to be functional, following which cysteine residues were introduced into predicted loops. HeLa cells, transiently transfected with these PCFT mutants, were then labeled with an impermeant, cysteine-specific biotinylation reagent (MTSEA-biotin) with or without permeabilization of cells. The biotinylated proteins were precipitated by streptavidin beads and assessed by Western blotting analysis. The biotinylation of PCFT was further confirmed by blocking cysteine residues with impermeant 2-sulfonatoethyl methanethiosulfonate. Two extracellular cysteine residues (66, 298) present in WT-PCFT were not biotinylated; however, in the absence of either one, biotinylation occurred. Likewise, biotinylation occurred after treatment with β-mercaptoethanol. Taken together, these analyses establish a PCFT secondary structure of 12 transmembrane domains with the N- and C- termini directed to the cytoplasm. The data indicate further that there is a disulfide bridge, which is not required for function, between the native C66 and C298 residues in the first and fourth transmembrane domains, respectively.

The proton-coupled folate transporter (PCFT;[1] SLC46A1; NP_54200) was recently cloned and its critical role in intestinal absorption of folate vitamins established by this laboratory with the demonstration of loss-of-function mutations in the *pcft* gene in six unrelated families with the autosomal recessive disorder, hereditary folate malabsorption (HFM) (*1*, *2*). Since then, four additional subjects with the clinical diagnosis of HFM were shown to have mutations in this gene (*3*−*6*). PCFT also plays a critical role in transport of folates into the central nervous system since patients with HFM have very low folate levels in the cerebrospinal fluid (*7*, *8*) (GeneReviews, http://www.ncbi.nlm.nih.gov/bookshelf/br.fcgi?book = gene&part = folate-mal). PCFT-mediated folate transport is electrogenic, optimal at low pH, and is accompanied by intracellular acidification (*1*, *9*−*12*).

PCFT mediates antifolate absorption within the acidic microenvironment of the proximal small intestine. This is a particularly important route of administration for methotrexate in the treatment of autoimmune disorders, such as rheumatoid arthritis (*13*, *14*). PCFT plays an important role in pemetrexed transport into tumor cells (*11*); this is a novel antifolate approved for the treatment of pleural mesothelioma and nonsmall cell lung cancer (*15*−*19*). PCFT has a very high affinity for pemetrexed at the transporter's optimal low pH and retains a much higher affinity for this drug than other antifolates even at neutral pH, in the absence of a pH gradient, driven by the transmembrane voltage gradient (*1*, *11*). Hence, in the absence of the reduced folate carrier (SLC19A1), the major facilitative folate transporter that functions optimally at pH 7.4, pemetrexed transport is substantially preserved while transport of other antifolates, such as methotrexe, is impaired. This results in retention of pemetrexed activity even when there is intrinsic or acquired resistance to methotrexate on this basis (*20*−*22*).

Based upon immunohistochemical analyses, both the N- and C-termini of human and rodent PCFT are located within the cytoplasm consistent with an even number of transmembrane helices (*10*, *23*). The subsequent demonstration that two predicted N-linked glycosylation sites are, in fact, glycosylated in human PCFT provided additional evidence for the extracellular location of the loop between the first and second TMDs (*23*). In the current paper, the substituted cysteine accessibility method (SCAM) was utilized to further characterize the membrane topology of PCFT (*24*). First, a functional cysteineless PCFT (CL-PCFT) was generated, following which residues in predicted external and internal loops were replaced with cysteine, and the accessibility of the residues probed with a methanethiosulfonate-biotin reagent in the presence or absence of membrane permeabilization. The results provide evidence for a 12 TMD topology and an interaction between two native cysteine residues localized in extracellular loops.

†This work was supported by grants from the National Institutes of Health, CA-82621, and the Mesothelioma Applied Research Foundation.

*Corresponding author. Tel: 718-430-2302. Fax: 718-430-8550. E-mail: igoldman@aecom.yu.edu.

[1]Abbreviations: CL, cysteineless; EL, extracellular loop; IL, intracellular loop; TMD, transmembrane domain; MTSEA-biotin, (2-((biotinoyl)amino)ethyl methanethiosulfonate; MTSES, 2-sulfonatoethyl methanethiosulfonate; DTT, dithiothreitol; PCFT, the proton-coupled folate transporter; SCAM, substituted cysteine accessibility method; HFM, hereditary folate malabsorption.

Published on Web 03/03/2010

Table 1: Sense Primers for Generation of Human PCFT Mutants Used in the Current Study

mutations	primer sequence (5′ to 3′)
C21S	GCGGCTGCCGTGCTGTCCCGGGGCCCGGTAGAG
C66S	CGCCAAAGGGGGGGCTCCAGCAACCGCAGCGCG
C151S	CTGGGTCGCATCCTTTCTGCCCTCCTCGGCGAC
C229S	CTCTATGCAGCTTTCTCCTTTGGTGAGACCTTA
C298S	CTAAGCACACCCCTCTCCTGGGACTCCAAACTA
C328S	AAGCTCCTGCAGTACTCCCTGGCCGATGCCTGG
C397S	TTTTCTGCTGTGGCCTCTGTGAAATAGCCTGGCC
S110C	GGAGC TTGGAGCGAC TGTGTGGGCCGCCGCCCG
V141C	CAGCTGCAGCTCCACTGCGGCTACTTCGTGCTG
S174C	GATGTCAGCTCCTGCCGCAGCCGCACC
G207C	TGGCTCCGGGCCCAGTGTTATGCCAACCCCTTC
T240C	GAGCCAAAGTCCTGCCGGCTCTTCAC
E261C	GCTCCCGCCCCATGCAAGTCCAGGAAA
E292C	TTAACCCTTTATTGCCTAAGCACACCC
L329C	CTGCAGTACTCCTGCGCCGATGCCTGG
L357C	GCCACTATCACGCCTTGCATGTTCACAGGATAT
T386C	AAGCTGGTGAGAGAGTGCGAGCAGGGTGCTCTC
T417C	TCACTCTACCCAGCCTGTCTGAACTTTATGAAG

MATERIALS AND METHODS

Generation of PCFT Mutant Expression Vectors by Site-Directed Mutagenesis. The construction of a C-terminal HA- (hemagglutinin-) tagged human PCFT expression vector has been described (*23*). All PCFT mutants generated for this study were HA-tagged at the C-terminus. The CL-PCFT expression vector was generated in two steps with the QuikChange multisite-directed mutagenesis kit (Stratagene, La Jolla, CA). In the first step, C21, C66, and C151 were simultaneously replaced with serine, and in the second step, C229, C298, C328, and C397 were simultaneously changed to serine. The primers used in these procedures are listed in Table 1. For introduction of cysteine residues into CL-PCFT, the QuikChange II XL site-directed mutagenesis kit (Stratagene, La Jolla, CA) was utilized. The sense primers for these mutations are listed in Table 1. For some mutations a temperature (50 °C) lower than the standard annealing temperature of 60 °C was required. The coding region of the final expression vectors was verified by automated sequencing in the Albert Einstein Cancer Center Genomics Shared Resource.

Cell Lines and Chemicals. HeLa cells were maintained in RPMI-1640 medium supplemented with 10% fetal bovine serum, 100 units/mL penicillin, and 100 μg/mL streptomycin. [3′,5′,7-^{3}H-(N)]Methotrexate was purchased from Moravek Biochemicals (Brea, CA). Other reagents utilized for SCAM are indicated below in the description of the specific methodologies.

Transport Measurements. HeLa cells were seeded into 20 mL low background glass scintillation vials (Research Products International Corp., Prospect, IL) at a density of 0.4 million cells/vial. The next day, cells were transfected with PCFT expression vectors (1 μg/vial) and Lipofectamine 2000 (2.5 μL/vial; Invitrogen, Carlsbad, CA) according to the manufacturer's protocol. [^{3}H]Methotrexate influx was assessed 2 days after transfection. Briefly, cells were washed twice with HBS (20 mM HEPES, 5 mM dextrose, 140 mM NaCl, 5 mM KCl, 2 mM $MgCl_2$, pH 7.4) and incubated in the same buffer at 37 °C for 20 min. The incubation buffer was then aspirated, and transport was initiated by the addition of 0.5 mL of prewarmed (37 °C) MBS (20 mM MES, 140 mM NaCl, 5 mM KCl, 2 mM $MgCl_2$, pH 5.5) containing 0.5 μM [^{3}H]methotrexate. Uptake was carried out at 37 °C over 2 min, which approximated initial rates under these conditions, and stopped by the addition of 5 mL of ice-cold HBS. Cells were washed three times with ice-cold HBS and dissolved in 0.5 mL of 0.2 M NaOH at 65 °C for 40 min. Radioactivity in 0.4 mL of lysate was measured on a liquid scintillation spectrometer and normalized to protein levels obtained with the BCA protein assay (Pierce, Rockford, IL).

Biotinylation and Immunoprecipitation. HeLa cells were seeded in six-well plates at a density of 0.6 million cells per well. On day 2, cells were transfected according to the manufacturer's protocol with HA-tagged PCFT expression vectors (2 μg/well) and Lipofectamine 2000 (5 μL/well). The serum-free RPMI-1640 medium employed in the transfection protocol was replaced with normal growth medium 4 h later. On day 3, the growth medium was replaced with fresh medium. Biotinylation was conducted on the fourth day with MTSEA-biotin (Biotium, Hayward, CA). MTSEA-biotin was dissolved in DMSO at a concentration of 2 mg/100 μL and then diluted with PBS at a ratio of 1 to 100. Cells that had been washed twice with 2 mL of PBS were immediately incubated with this MTSEA-biotin solution (1 mL/well) for 30 min at room temperature. The MTSEA-biotin solution was aspirated, and the cells were washed twice with 2 mL of PBS and then overlaid on ice with 0.7 mL of hypotonic buffer (0.5 mM Na_2HPO_4, 0.1 mM EDTA, pH 7.0) containing protease inhibitor cocktail (Roche, Indianapolis, IN). The cells were then detached from the plates with disposable cell lifters and centrifuged at 16000*g* and 4 °C for 5 min. The pellet was then resuspended in 0.4 mL of lysis buffer (50 mM Tris−base, 150 mM NaCl, 1% NP40, 0.5% sodium deoxycholate, pH 7.4) and mixed on a rotisserie shaker for 1 h at 4 °C before recentrifugation at 16000*g* and 4 °C for 15 min. The supernatant was collected and identified as "crude membrane fraction"; 25 μL of this fraction was separated and stored at −20 °C. The remaining crude membrane fraction (~375 μL) was mixed on a rotisserie shaker overnight at 4 °C with 50 μL of streptavidin−agarose resin (Thermo Scientific, Rockford, IL) that was prewashed three times with the lysis buffer. The next day (day 5), the mixture was centrifuged for 30 s at 16000*g* following which the supernatant was aspirated from the resin which was then washed three times with the 0.5 mL of lysis buffer, each with a 20 min mix on a rotisserie shaker. The final wash was with the lysis buffer supplemented with 2% SDS. The precipitated proteins were released from the resin by heating at 95 °C for 5 min in 2× SDS−PAGE sample loading buffer containing dithiothreitol (DTT).

To optimize permeabilization, cells were initially incubated with different concentrations of digitonin in PBS for 5 min (*25*). A concentration of digitonin of 50 μg/mL was the minimum level required to permeabilize ~75% of HeLa cells (assayed by trypan blue exclusion) and was used in all studies. While a higher concentration of digitonin achieved greater permeabilization, this resulted in increased nonspecific binding of proteins to the streptavidin−agarose resin. To block cysteine residues with MTSES (Toronto Research Chemicals Inc., Canada), a concentration of 1 mg/mL of this reagent in PBS was prepared and immediately added (1 mL/well) to prewashed cells and incubated at room temperature for 30 min. To disrupt the disulfide bridge, cells expressing WT-PCFT were treated with 20 mM β-mercaptoethanol in PBS for 30 min at room temperature followed by two washes with PBS.

Western Blotting Analysis. All samples were resolved on standard 12.5% SDS−PAGE without reducing reagent. The precipitated proteins (released from beads as described in see previous sections) were loaded directly on gels while the crude

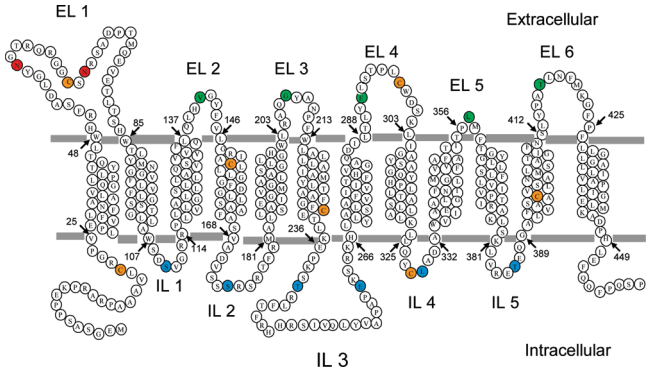

FIGURE 1: Membrane topology of human PCFT. A predicted model of the secondary structure of human PCFT (HMMTOP) supported by earlier reports (*10*, *23*) and the current study. Orange circles indicate seven native cysteine residues that were substituted with serine to obtain the cysteineless protein, CL-PCFT. Green circles mark residues that could be biotinylated without membrane permeabilization while blue circles indicate residues that could be biotinylated only after membrane permeabilization. Red circles indicate sites of N-glycosylation. EL, extracellular loop; IL, intracellular loop.

membranes were mixed (1:1) with DTT-containing 2× SDS−PAGE sample loading buffer at room temperature before loading on gels. After SDS−PAGE, proteins were transferred to Amersham Hybond membranes (GE Healthcare, Piscataway, NJ). The membranes were blocked with 10% dry milk in TBST (20 mM Tris, 135 mM NaCl, 1% Tween 20, pH 7.6) overnight and probed for 2 h with a rabbit anti-HA antibody (H6908; Sigma, St. Louis, MO) at a dilution of 1:5000 in TBST containing 0.1% dry milk. After three washes with TBST, membranes were incubated for 1 h on a shaker with anti-rabbit IgG-HRP conjugate (Cell Signaling Technology) in TBST at a 1:5000 dilution. After three additional washes with TBST, the blots were developed with Amersham ECL Plus reagent (GE Healthcare, Piscataway, NJ) and exposed to autoradiography film (Denville Scientific, Metuchen, NJ).

RESULTS

A Working Model of Human PCFT Membrane Topology. Different computer programs used by different servers predict a different number of transmenbrane domains (TMDs) for human PCFT topology. For example, 12-, 11-, or 10-TMD models are predicted by HMMTOP (*26*), TMHMM (*27*), or TMpred (*28*), respectively. Based upon the findings that both C- and N-termini are localized intracellularly and both predicted N-glycosylation sites (N58 and N68) are actually glycosylated, an even number of TMDs was required, and a 12-TMD topology was utilized as a working model for the current study (Figure 1).

Generation of Cysteineless Human PCFT. There are seven cysteine residues in human PFCT (Figure 1); their exact positions are indicated in Table 1. All of these residues were replaced with serine to generate a cysteineless PCFT or CL-PCFT. As indicated in Figure 2, [^{3}H]methotrexate influx mediated by CL-PCFT was ~85% that of WT-PCFT, a difference that did not reach statistical significance based upon the average of six independent experiments.

Introduction of Cysteine Residues in Loops Predicted To Be Extracellular or Intracellular in the CL-PCFT. Since the locations of the N- and C-termini as well as the first predicted extracellular loop (EL1) are established, the current study focused on predicted extracellular loops, EL 2 to EL 6, and

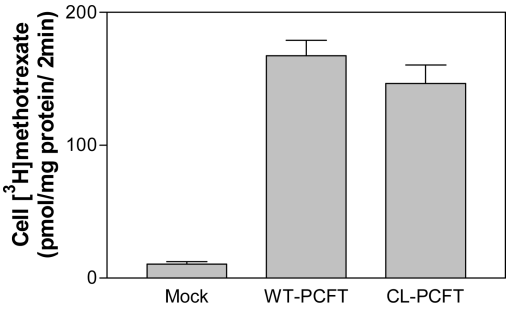

FIGURE 2: Assessment of CL-PCFT activity. CL-PCFT and WT-PCFT expression vectors were transiently transfected into HeLa cells. PCFT activity was determined 48 h later by assessment of [^{3}H]methotrexate influx (0.5 μM) at pH 5.5 over 2 min. Data are the mean ± SEM from six independent experiments.

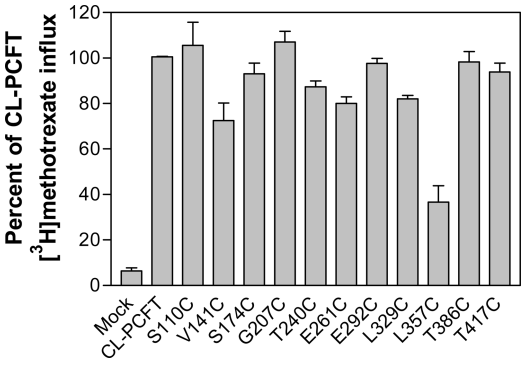

FIGURE 3: Assessment of transport activities of PCFT mutants generated for topological studies. CL-PCFT and mutant expression vectors were transiently transfected into HeLa cells. PCFT transport activities were assessed by 0.5 μM [^{3}H]methotrexate influx over 2 min at pH 5.5. The data for each mutant are expressed as percentage of CL-PCFT activity. The results are the mean ± SEM from three independent experiments.

predicted intracellular loops (IL), IL 1 to IL 5 (Figure 1). One residue in each targeted loop, except IL 3, was mutated to cysteine. Two residues in IL 3 were individually mutated to cysteine due to the large size of this loop (Figure 1 and Table 1). The resulting mutants met two basic requirements of SCAM. (i) The mutated PCFT retained function. (ii) The mutated PCFT could be labeled either in the absence or presence of membrane permeabilization.

Transport function for each PCFT mutant was assessed. As indicated in Figure 3, the majority of the mutant PCFTs had [^{3}H]methotrexate influx activities similar to, or slightly less than, that of CL-PCFT. Activity of the L357C mutant was 38% of CL-PCFT; this was far higher than that of the mock-transfected cells.

Biotinylation of PCFT Mutants with MTSEA-Biotin in the Absence of Permeabilization. Biotinylation of PCFT mutants was carried out with a membrane-impermeant reagent, MTSEA-biotin, in the absence of permeabilization. Under these conditions, only externally accessible cysteine residues can be labeled. As indicated in Figure 4, panel A, upper bands, V141C (EL 2), G207C (EL 3), E292C (EL 4), L357C (EL 5), and T417C (EL 6) mutants were labeled by MTSEA-biotin. CL-PCFT was not labeled as expected. It is interesting to note that WT-PCFT was also not labeled, despite the presence of two (C66, EL 1; C298, EL 4) extracellular cysteine residues (Figure 1). As a control, the amount of PCFT protein in the crude membrane preparation was also monitored (panel A, lower bands). Consistent with the lower transport activity, L357C protein in the

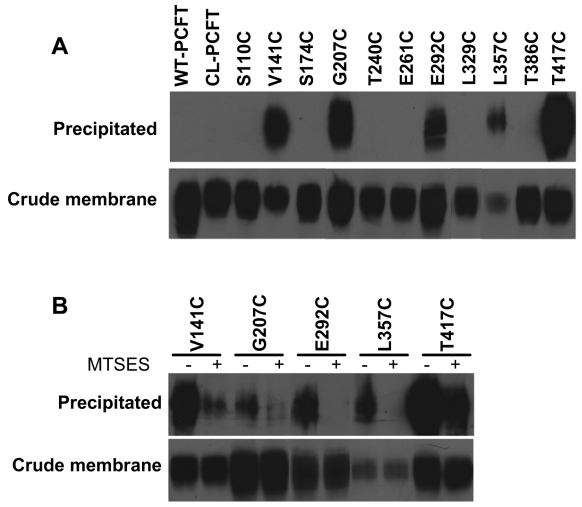

FIGURE 4: Bioinylation of PCFT mutants with MTSEA-biotin in the absence of permeabilization. HeLa cells transiently expressing HA-tagged WT-PCFT, CL-PCFT, or PCFT mutants were treated with MTSEA-biotin, and the crude membranes were then incubated with streptavidin beads to pull down biotinylated proteins. The proteins on the beads were recovered and analyzed by Western blot using an anti-HA antibody. PCFT protein in the crude membrane preparation was also analyzed to determine protein expression. Panel A: Representative labeling of PCFT expressed in HeLa cells with MTSEA-biotin in the absence of membrane permeabilization (upper bands) along with total PCFT protein in crude membrane (lower panel). Panel B: Effect of pretreatment with MTSES on biotinylation. The cells were either subjected directly to biotinylation or treated with MTSES before biotinylation. For both panels, at least two independent experiments were performed for each mutant, and the crude membrane sample was always matched to the precipitated sample.

crude membrane preparation was less than that of CL-PCFT. For all mutants as well as WT-PCFT, protein migrates as a broad band on SDS−PAGE between 60 and 80 kDa, consistent with N-glycosylation of this transporter (*23*).

If cysteine residues in V141C, G207C, E292C, L357C, and T417C mutants are indeed externally accessible, they should react with a cysteine-specific membrane-impermeant reagent, MTSES, thereby blocking subsequent biotinylation of these residues by MTSEA-biotin. As indicated in panel B of Figure 4, pretreatment of intact cells expressing these mutants with MTSES reduced, or near completely eliminated, their subsequent biotinylation. These results further confirm the extracellular accessibility of these residues. There was no signal at all observed for CL-PCFT, indicating that the labeling is highly specific.

Biotinylation of PCFT Mutants with MTSEA-Biotin after Membrane Permeabilization. The remaining mutants, that could not be labeled by MTSEA-biotin in the absence of permeabilization, were then treated with this reagent after cells were permeabilized with digitonin. As indicated in panel A of Figure 5, S110C (IL 1), S174C (IL 2), T240C (IL 3), E261C (IL 3), L329C (IL 4), and T386C (IL 5) were labeled under these conditions, consistent with the intracellular localization of these residues.

Panel B of Figure 5 confirms the intracellular location of cysteine residues in S110C, S174C, T240C, E261C, L329C, and T386 mutants. Condition "1" indicates standard biotinylation after permeabilization with digitonin, the same condition as described for panel A of this figure. Under condition "2", the intact cells were first treated with MTSES, the membrane-impermeant, cysteine-specific reagent followed by permeabilization of cells with digitonin before biotinylation with MTSEA-biotin.

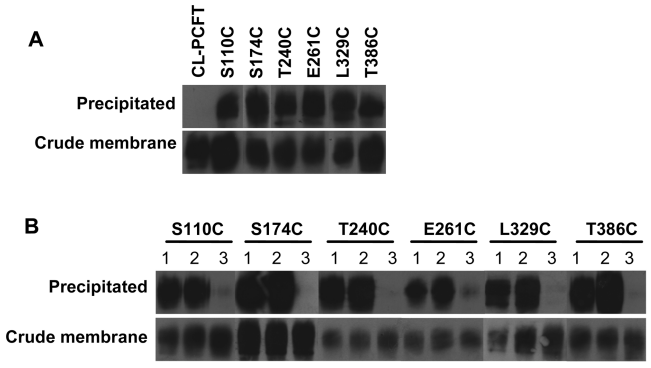

FIGURE 5: Biotinylation of PCFT mutants with MTSEA-biotin after permeabilization. Panel A: HeLa cells transiently expressing CL-PCFT or various mutants were permeabilized with digitonin before the biotinylation reaction. Panel B: Dependence of biotinylation inhibition by MTSES on digitonin permeabilization. Three conditions of biotinylation labeling were conducted for each mutant: (1) Cells were permeabilized before the biotinylation reaction (same as described for panel A of this figure). (2) Cells were first treated with MTSES and then permeabilized with digitinon before the biotinylation reaction. (3) Cells were permeabilized with digitonin first and then treated with MTSES before the biotinylation reaction. For all panels, the crude membrane sample was matched to the precipitated sample, and results are representative of at least two separate experiments.

Since MTSES does not diffuse into cells, intracellularly localized cysteine residues should not be blocked, and biotinylation should not be affected. This was what was observed. Under condition "3", cells were first permeabilized with digitonin and then treated with MTSES followed by biotinylation with MTSEA-biotin. Under this condition, the cells were permeable to MTSES resulting in its reaction with intracellularly localized cysteine residues thereby blocking the subsequent biotinylation of the mutants.

Identification of an Intermolecular Disulfide Bridge between Native Cysteine 66 and Cysteine 298 Residues in Human PCFT. As indicated above, WT-PCFT was not labeled with MTSEA-biotin in the absence of membrane permealization despite the fact that two native cysteine residues, C66 and C298, were localized to EL 1 and EL 4, respectively. One explanation for this finding is that both cysteine residues were not accessible to labeling reagent due to steric hindrance. Another possibility is that these residues form a disulfide bridge and thus neither sulfhydryl group is available for the labeling reaction. The following studies were designed to test these possibilities.

First, cells expressing WT-PCFT were treated with β-mercaptoethanol to disrupt a potential disulfide bridge thereby releasing sulfhydryl groups. As indicated in panel A of Figure 6, pretreatment of cells with β-mercaptoethanol resulted in labeling of WT-PCFT with MTSEA-biotin in the absence of permealization. Next, C66, C298, or both residues in WT-PCFT were substituted with serine to generate C66S, C298S, and C66S/C298S mutants. As expected, the activities of C66S, C298S, or C66S/C298S, assessed by [^{3}H]methotrexate influx, were comparable to that of WT-PCFT (95 $\pm$ 5%, 90 $\pm$ 1%, or 96 $\pm$ 5% of WT-PCFT activity, respectively, based upon three independent experiments). As indicated in panel B of Figure 6, replacement of either C66 or C298 with serine allowed PCFT to be labeled by MTSEA-biotin, indicating that elimination of one cysteine of the disulfide bridge frees the other cysteine for the reaction. When both cysteine residues were removed from WT-PCFT, the mutant was not labeled by the MTSEA-biotin. Hence, these data are consistent with the presence of a disulfide bond between

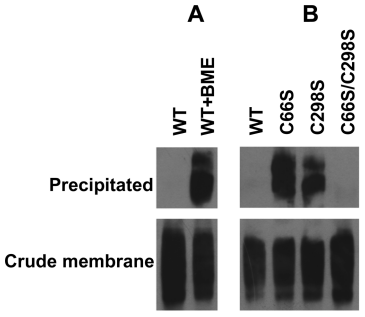

FIGURE 6: Identification of a disulfide bond between C66 and C298 in human PCFT. Panel A: The effect of treatment with 20 mM β-mercaptoethanol (BME) on biotinylation of HeLa cells expressing WT-PCFT. Panel B: Biotinylation of WT-PCFT and mutants in which C66, C298, or both were replaced with serine. For both panels, at least two independent experiments were performed for each mutant, and the crude membrane sample was always matched to the precipitated sample.

the C66 and C298 residues. It is of interest that PCFT protein migrates on SDS−PAGE as distinct double bands (Figure 6) in the absence of the disulfide bond as compared to a single band in the presence of the disulfide bond (Figures 4 and 5).

Additional studies were designed to determine whether the disulfide bridge is intra- or intermolecular; in the latter case the bond would represent the formation of a dimer or polymer among two or more PCFT molecules. If the disulfide bond is formed intermolecularly, the molecular size of PCFT would be twice that of the monomer or higher and would migrate much slower on SDS−PAGE in the absence any reducing reagent. WT-PCFT, C66S, C298C, and C66S/C298S mutants were thus treated with the SDS−PAGE sample buffer in the absence of DTT along with a control where the treatment was performed in the presence of DTT to disrupt the disulfide bond. No change in migration was seen on SDS−PAGE under these two conditions for WT-PCFT, indicating the absence of an intermolecular disulfide bond in WT-PCFT (data not shown). In addition, the migration pattern for C66S, C298S, and C66/C298 mutants was the same as WT-PCFT, regardless of the presence of DTT. Hence, the disulfide bridge formed between C66 and C298 is intramolecular.

DISCUSSION

The current study utilized SCAM to define the localization of loops connecting PCFT transmembrane domains, an approach that has been applied to thoroughly characterize structural aspects of the reduced folate carrier (SLC19A1), the other major facilitative folate transport carrier (*29*−*31*). These data along with earlier immunohistochemical localization of the N- and C- termini of the human and murine PCFT within the cytoplasm indicate a PCFT topology consisting of 12 transmembrane domains. This is different than an earlier model of this carrier suggesting 9 TMDs with the C-terminus localized extracellularly (*32*). Of course, ultimate resolution of the topology and three-dimensional structure of PCFT will require a high-resolution crystal structure which has not as yet been achieved for a eukaryotic transporter.

The localization of two cysteine mutants (T240C and E261C), inserted near the membrane−aqueous boundaries of the large central loop (IL 3), to the intracellular compartment confirms the location of the fully conserved H247 residue. Likewise, the results with the S174C mutant confirm the location of the fully conserved S172 at IL 2. Homology modeling predicted, and site-directed mutagenesis supported, the likelihood that these residues are in hydrogen bond distance and influence the accessibility of folate substrates to the binding pocket within the translocation pathway (*9*). The integrity of the association between these two residues was also shown to limit proton slippage through the PCFT aqueous translocation pathway independent of folate substrate transport (*9*). Likewise, the data confirm the location of H281 in the seventh TMD, a residue that appears to influence proton binding which, in turn, modulates folate binding (*9*). The E185 residue, which plays an important role in proton coupling, is confirmed to reside as predicted, in the fifth TMD (*33*). Confirmation of the secondary structure also strengthens localization of other PCFT residues mutated in patients with HFM (*2*, *5*).

The observation that two native cysteine residues, C66 and C298, in WT-PCFT could not be labeled by MTSEA-biotin in spite of their extracellular location led to identification of an intramolecular disulfide bridge between these two residues. Apparently, the formation of this disulfide bond is not critical to PCFT function since the C66S, C289S, and C66S/C298S mutants and even CL-PCFT have transport activities comparable to that of WT- PCFT. This is in contrast to the more important role disulfide bridges play in other transporters. For example, the intramolecular bridge between C592 and C608 in the multidrug resistance-associated protein, ABCG2, is critical for membrane targeting and function (*34*). The disulfide bridge between C180 and C329 in the human proton-coupled amino acid transporter, hPAT1, is required for substrate binding (*35*). Disruption of the disulfide bond between C126 and C333 in the human vesicle monoamine transporter (VMAT2) impairs transport function (*36*). Elimination of the bridge between C255 and C511 in the human sodium/glucose cotransporter (SGT1) alters conformation of the transporter and decreases its affinity for α-methylglucose (*37*). All cysteine-associated disulfides bridges, as described above, are located extracellularly.

In the absence of a crystal structure, homology models have been employed to characterize eukaryotic facilitative transporters based upon the known structures of bacterial transporters (*38*). In the case of human PCFT, its structure has been predicted using the template of the bacterial glycerol 3-phosphate transporter: GlpT (*5*, *9*). The results from the current study not only verify the 12-transmembrane domain topology of human PCFT but also provide new structural information that will allow refinement of the homology model. Hence, the substituted residues in the extracellular and intracellular loop must be exposed to their respective aqueous compartments since they are fully accessible to the MTSEA-biotin. Further, the native cysteine 66 in EL 1 must be physically close to cysteine 298 in EL 4 within the context of the tertiary structure since these two residues form a disulfide bridge.

Other approaches to determine transporter topology utilize insertion of an immunoreactive epitope or N-glycosylation site. For example, along with SCAM (*29*), insertion of hemagglutinin (HA) (*39*, *40*) and N-glycosylation (*40*) sites has been used to determine the topology of human reduced folate carrier. Major advantages of SCAM include minimal structural effects associated with cysteine substitutions as well as rapid and selective reaction of the cysteine sulfhydryl group. Epitope insertion requires introduction of multiple sequential amino acid residues in a transporter, an alteration that may affect transport function. Also, an antibody is much more likely to be inaccessible to the

epitope then the much smaller sulfhydryl reagents. For N-glycosylation scanning mutagenesis, a predicted N-glycosylation site (NXS/T) may not be glycosylated, even if it is extracellularly located, if the targeted loop is small. Also, this approach cannot be used for localization of intracellular loops.

ACKNOWLEDGMENT

We are grateful to Dr. Myles H. Akabas for helpful suggestions.

REFERENCES

1. Qiu, A., Jansen, M., Sakaris, A., Min, S. H., Chattopadhyay, S., Tsai, E., Sandoval, C., Zhao, R., Akabas, M. H., and Goldman, I. D. (2006) Identification of an intestinal folate transporter and the molecular basis for hereditary folate malabsorption. *Cell 127*, 917–928.
2. Zhao, R., Min, S. H., Qiu, A., Sakaris, A., Goldberg, G. L., Sandoval, C., Malatack, J. J., Rosenblatt, D. S., and Goldman, I. D. (2007) The spectrum of mutations in the PCFT gene, coding for an intestinal folate transporter, that are the basis for hereditary folate malabsorption. *Blood. 110*, 1147–1152.
3. Min, S. H., OH, S. Y., Karp, G. I., Poncz, M., Zhao, R., and Goldman, I. D. (2008) The clinical course and genetic defect in the PCFT in a 27-year-old woman with hereditary folate malabsorption. *J. Pediatr. 153*, 435–437.
4. Meyer, E., Kurian, M. A., Pasha, S., Trembath, R. C., Cole, T., and Maher, E. R. (2009) A novel PCFT gene mutation (p.Cys66LeufsX99) causing hereditary folate malabsorption, Mol. Genet. Metab. (Epub ahead of print).
5. Lasry, I., Berman, B., Straussberg, R., Sofer, Y., Bessler, H., Sharkia, M., Glaser, F., Jansen, G., Drori, S., and Assaraf, Y. G. (2008) A novel loss of function mutation in the proton-coupled folate transporter from a patient with hereditary folate malabsorption reveals that Arg 113 is crucial for function. *Blood 112*, 2055–2061.
6. Borzutzky, A., Crompton, B., Bergmann, A. K., Giliani, S., Baxi, S., Martin, M., Neufeld, E. J., and Notarangelo, L. D. (2009) Reversible severe combined immunodeficiency phenotype secondary to a mutation of the proton-coupled folate transporter. *Clin. Immunol. 133*, 287–294.
7. Geller, J., Kronn, D., Jayabose, S., and Sandoval, C. (2002) Hereditary folate malabsorption: family report and review of the literature. *Medicine* (*Baltimore*) *81*, 51–68.
8. Zhao, R., Matherly, L. H., and Goldman, I. D. (2009) Membrane transporters and folate homeostasis: intestinal absorption and transport into systemic compartments and tissues. *Expert Rev. Mol. Med. 11*, e4.
9. Unal, E. S., Zhao, R., Chang, M. H., Fiser, A., Romero, M. F., and Goldman, I. D. (2009) The functional roles of the His247 and His281 residues in folate and proton translocation mediated by the human proton-coupled folate transporter SLC46A1. *J. Biol. Chem. 284*, 17846–17857.
10. Qiu, A., Min, S. H., Jansen, M., Malhotra, U., Tsai, E., Cabelof, D. C., Matherly, L. H., Zhao, R., Akabas, M. H., and Goldman, I. D. (2007) Rodent intestinal folate transporters (SLC46A1): secondary structure, functional properties, and response to dietary folate restriction. *Am. J. Physiol. Cell Physiol. 293*, C1669–C1678.
11. Zhao, R., Qiu, A., Tsai, E., Jansen, M., Akabas, M. H., and Goldman, I. D. (2008) The proton-coupled folate transporter (PCFT): impact on pemetrexed transport and on antifolate activities as compared to the reduced folate carrier. *Mol. Pharmacol. 74*, 854–862.
12. Umapathy, N. S., Gnana-Prakasam, J. P., Martin, P. M., Mysona, B., Dun, Y., Smith, S. B., Ganapathy, V., and Prasad, P. D. (2007) Cloning and functional characterization of the proton-coupled electrogenic folate transporter and analysis of its expression in retinal cell types. *Invest. Ophthalmol. Visual Sci. 48*, 5299–5305.
13. Cronstein, B. N. (2005) Low-dose methotrexate: a mainstay in the treatment of rheumatoid arthritis. *Pharmacol. Rev. 57*, 163–172.
14. Yokooji, T., Mori, N., and Murakami, T. (2009) Site-specific contribution of proton-coupled folate transporter/haem carrier protein 1 in the intestinal absorption of methotrexate in rats. *J. Pharm. Pharmacol. 61*, 911–918.
15. Chattopadhyay, S., Moran, R. G., and Goldman, I. D. (2007) Pemetrexed: biochemical and cellular pharmacology, mechanisms, and clinical applications. *Mol. Cancer Ther. 6*, 404–417.
16. Vogelzang, N. J., Rusthoven, J. J., Symanowski, J., Denham, C., Kaukel, E., Ruffie, P., Gatzemeier, U., Boyer, M., Emri, S., Manegold, C., Niyikiza, C., and Paoletti, P. (2003) Phase III study of pemetrexed in combination with cisplatin versus cisplatin alone in patients with malignant pleural mesothelioma. *J. Clin. Oncol. 21*, 2636–2644.
17. Hanna, N., Shepherd, F. A., Fossella, F. V., Pereira, J. R., De Marinis, F., Von Pawel, J., Gatzemeier, U., Tsao, T. C., Pless, M., Muller, T., Lim, H. L., Desch, C., Szondy, K., Gervais, R., Shaharyar, Manegold, C., Paul, S., Paoletti, P., Einhorn, L., and Bunn, P. A., Jr. (2004) Randomized phase III trial of pemetrexed versus docetaxel in patients with non-small-cell lung cancer previously treated with chemotherapy. *J. Clin. Oncol. 22*, 1589–1597.
18. Scagliotti, G. V., Parikh, P., Von Pawel, J., Biesma, B., Vansteenkiste, J., Manegold, C., Serwatowski, P., Gatzemeier, U., Digumarti, R., Zukin, M., Lee, J. S., Mellemgaard, A., Park, K., Patil, S., Rolski, J., Goksel, T., De Marinis, F., Simms, L., Sugarman, K. P., and Gandara, D. (2008) Phase III study comparing cisplatin plus gemcitabine with cisplatin plus pemetrexed in chemotherapy-naive patients with advanced-stage non-small-cell lung cancer. *J. Clin. Oncol. 26*, 3543–3551.
19. Ciuleanu, T., Brodowicz, T., Zielinski, C., Kim, J. H., Krzakowski, M., Laack, E., Wu, Y. L., Bover, I., Begbie, S., Tzekova, V., Cucevic, B., Pereira, J. R., Yang, S. H., Madhavan, J., Sugarman, K. P., Peterson, P., John, W. J., Krejcy, K., and Belani, C. P. (2009) Maintenance pemetrexed plus best supportive care versus placebo plus best supportive care for non-small-cell lung cancer: a randomised, double-blind, phase 3 study. *Lancet 374*, 1432–1440.
20. Zhao, R., and Goldman, I. D. (2003) Resistance to antifolates. *Oncogene 22*, 7431–7457.
21. Chattopadhyay, S., Zhao, R., Krupenko, S. A., Krupenko, N., and Goldman, I. D. (2006) The inverse relationship between reduced folate carrier function and pemetrexed activity in a human colon cancer cell line. *Mol. Cancer Ther. 5*, 438–449.
22. Zhao, R., Hanscom, M., Chattopadhyay, S., and Goldman, I. D. (2004) Selective preservation of pemetrexed pharmacological activity in HeLa cells lacking the reduced folate carrier; association with the presence of a secondary transport pathway. *Cancer Res. 64*, 3313–3319.
23. Unal, E. S., Zhao, R., Qiu, A., and Goldman, I. D. (2008) N-linked glycosylation and its impact on the electrophoretic mobility and function of the human proton-coupled folate transporter (HsPCFT). *Biochim. Biophys. Acta 1178*, 1407–1414.
24. Karlin, A., and Akabas, M. H. (1998) Substituted-cysteine accessibility method. *Methods Enzymol. 293*, 123–145.
25. Chen, J. G., Liu-Chen, S., and Rudnick, G. (1998) Determination of external loop topology in the serotonin transporter by site-directed chemical labeling. *J. Biol. Chem. 273*, 12675–12681.
26. Tusnady, G. E., and Simon, I. (1998) Principles governing amino acid composition of integral membrane proteins: application to topology prediction. *J. Mol. Biol. 283*, 489–506.
27. Krogh, A., Larsson, B., von Heijne, G., and Sonnhammer, E. L. (2001) Predicting transmembrane protein topology with a hidden Markov model: application to complete genomes. *J. Mol. Biol. 305*, 567–580.
28. Hofmann, K., and Stoffel, W. (1993) TMbase—A database of membrane spanning proteins segments. *Biol. Chem. Hoppe Seyler 374*, 166.
29. Cao, W., and Matherly, L. H. (2004) Analysis of the membrane topology for transmembrane domains 7−12 of the human reduced folate carrier by scanning cysteine accessibility methods. *Biochem. J. 378*, 201–206.
30. Hou, Z., Ye, J., Haska, C. L., and Matherly, L. H. (2006) Transmembrane domains 4, 5, 7, 8, and 10 of the human reduced folate carrier are important structural or functional components of the transmembrane channel for folate substrates. *J. Biol. Chem. 281*, 33588–33596.
31. Hou, Z., Stapels, S. E., Haska, C. L., and Matherly, L. H. (2005) Localization of a substrate binding domain of the human reduced folate carrier to transmembrane domain 11 by radioaffinity labeling and cysteine-substituted accessibility methods. *J. Biol. Chem. 280*, 36206–36213.
32. Shayeghi, M., Latunde-Dada, G. O., Oakhill, J. S., Laftah, A. H., Takeuchi, K., Halliday, N., Khan, Y., Warley, A., McCann, F. E., Hider, R. C., Frazer, D. M., Anderson, G. J., Vulpe, C. D., Simpson, R. J., and McKie, A. T. (2005) Identification of an intestinal heme transporter. *Cell 122*, 789–801.
33. Unal, E. S., Zhao, R., and Goldman, I. D. (2009) Role of the glutamate 185 residue in proton translocation mediated by the proton-coupled folate transporter SLC46A1. *Am. J. Physiol. Cell Physiol. 297*, C66–C74.

34. Henriksen, U., Fog, J. U., Litman, T., and Gether, U. (2005) Identification of intra- and intermolecular disulfide bridges in the multidrug resistance transporter ABCG2. *J. Biol. Chem. 280*, 36926–36934.
35. Dorn, M., Weiwad, M., Markwardt, F., Laug, L., Rudolph, R., Brandsch, M., and Bosse-Doenecke, E. (2009) Identification of a disulfide bridge essential for transport function of the human proton-coupled amino acid transporter hPAT1. *J. Biol. Chem. 284*, 22123–22132.
36. Thiriot, D. S., Sievert, M. K., and Ruoho, A. E. (2002) Identification of human vesicle monoamine transporter (VMAT2) lumenal cysteines that form an intramolecular disulfide bond. *Biochemistry 41*, 6346–6353.
37. Gagnon, D. G., Bissonnette, P., and Lapointe, J. Y. (2006) Identification of a disulfide bridge linking the fourth and the seventh extracellular loops of the Na^+/glucose cotransporter. *J. Gen. Physiol. 127*, 145–158.
38. Lemieux, M. J. (2007) Eukaryotic major facilitator superfamily transporter modeling based on the prokaryotic GlpT crystal structure. *Mol. Membr. Biol. 24*, 333–341.
39. Ferguson, P. L., and Flintoff, W. F. (1999) Topological and functional analysis of the human reduced folate carrier by hemagglutinin epitope insertion. *J. Biol. Chem. 274*, 16269–16278.
40. Liu, X., and Matherly, L. (2002) Analysis of membrane topology of the human reduced folate carrier protein by hemagglutinin epitope insertion and scanning glycosylation insertion mutagenesis. *Biochim. Biophys. Acta 1564*, 333–342.